Experimental study of surface-plasmon scattering by individual surface defects

Igor I. Smolyaninov and David L. Mazzoni
Electrical Engineering Department, University of Maryland, College Park, Maryland 20742

Joseph Mait
US Army Research Laboratory, AMSRL-SE-EO, 2800 Powder Mill Road, Adelphi, Maryland 20783

Christopher C. Davis
Electrical Engineering Department, University of Maryland, College Park, Maryland 20742
(Received 26 February 1997)

A direct-write ablation technique has been implemented in a photon scanning tunneling microscope setup. This combination allows us to study surface-plasmon (SP) scattering by *in situ* created individual surface defects, while the sizes and shapes of the defects are varied continuously. It is found that within a certain range of its size, a ''hill'' on an otherwise flat surface can be the source of a very narrow plasmon beam. This effect is explained using the Huygens-Fresnel principle. Shadowing and refraction of the SP field by smaller defects has also been observed. In order to explain these results we introduce an effective SP refractive index for two classes of surface defects: shallow topographical defects and areas covered with absorbed molecular layers. This concept allows us to achieve a qualitative understanding of plasmon scattering in many practical cases. Some simple optical elements for the control of SP propagation are suggested and demonstrated. Our observations suggest numerous practical applications in multichannel chemical sensing, biosensing, and integrated optics. [S0163-1829(97)05928-6]

I. INTRODUCTION

The surface plasmon (SP) is a fundamental electromagnetic excitation mode of a metal-dielectric interface.[1,2] The properties of SP's have been the subject of extensive studies because of their extreme sensitivity to surface roughness and the dielectric properties of surface absorbed layers. This sensitivity results from the exponential dependence of the SP electromagnetic field on the distance from the interface in each of the bounding media. The SP is free to propagate along the metal surface with a mean free path determined by the quality of the surface and Ohmic losses. If the surface is perfectly flat then Ohmic loss is the only channel for decay, since the momentum conservation law prohibits SP conversion into photons. In the visible range the SP mean free path on a silver surface is limited to about 50 μm but can extend to many mm in the infrared region.[3] Similar waves exist on the surfaces of a number of dielectrics and semiconductors.[1] Since the properties of SP's depend strongly on the properties of the interface along which they propagate, they have found applications in the surface-roughness analysis,[1] gas detection, and biosensing.[4]

Until recently there was no tool for the direct study of SP propagation, since the SP field decay length perpendicular to the interface is on the order of 100 nm in the visible range. Indirect information about SP properties had been extracted from far-field measurements of light scattered into a free space by SP interaction with surface defects such as in surface-plasmon microscopy.[5] The development of scanning probe techniques has opened the way to a study of SP properties at the surface along which the SP propagates with resolution in the nanometer range. The scanning tunneling microscopy (STM) was the first such technique. In STM experiments an additional tunneling current has been observed in the presence of the SP wave.[6] A closely related technique, in which the SP field scattered by a STM tip is detected in the far-field zone, has been introduced by Specht *et al.*[7] However, a metallic STM tip positioned within a fraction of a nanometer from the surface causes a very strong perturbation of the initial SP field distribution. The results of these experiments reflect the properties of localized plasmon modes[8] that develop between the STM tip and the sample rather than the unperturbed SP field distribution. Similarly an atomic force microscope (AFM) tip has been used to scatter the SP field.[9] Although less intrusive then STM, this technique also relies on the perturbation of the SP field as its sensitive mechanism. Kim *et al.* even refer to the potential benefits of a metal-coated AFM tip for obtaining an improvement in the sensitivity of this technique.[9]

The development of near-field optical microscopy[10] has created different ways for probing the SP field distribution. For example, in a tunneling near-field optical microscopy[11] light from a metal-coated optical fiber tip is used for SP excitation. However, the most successful experimental geometry for measuring the true unperturbed SP field distribution appears to be the photon scanning tunneling microscopy (PSTM).[12] In the PSTM geometry a fiber tip is used to detect the evanescent field of the light being totally internally reflected at the sample surface. In Ref. 13, PSTM was used to measure the exponential decay of the SP field away from a metal-air interface. SP propagation along the interface has also been studied[14] and the SP propagation length measured. SP's on both an external metal-air interface and an internal interface between a metal film and a glass substrate have been excited[15] and the SP field distribution for both modes has been mapped. Extension of SP studies to the control of

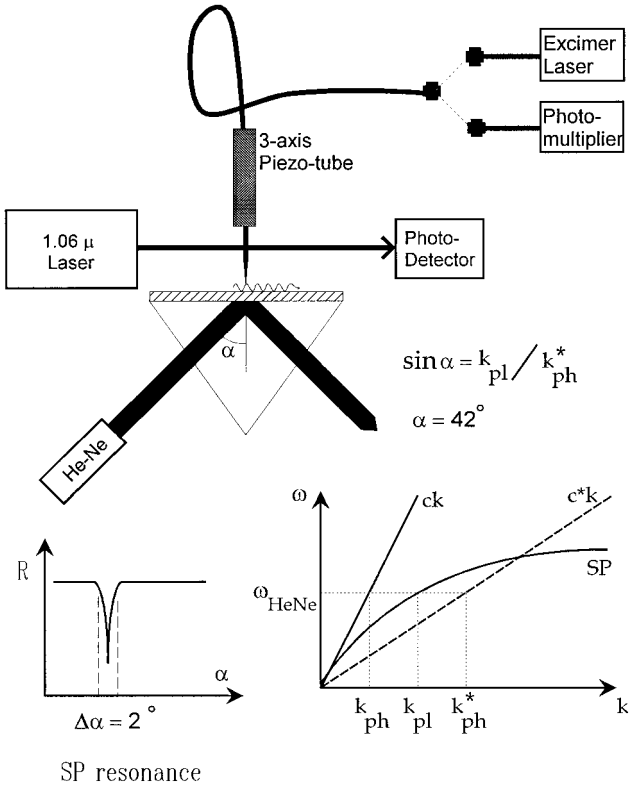

FIG. 1. Schematic view of the experimental setup. Dispersion curves for surface plasmons and photons in air and in glass are shown in the inset.

SP's by two-dimensional optics is anticipated. This could create numerous applications in integrated optics and multichannel chemical sensing and biosensing. However, until recently there has been no attempt to create a real two-dimensional optical element for SP's.

Recently we studied the scattering of SP's by *in situ* created individual surface defects.[16] Some prototype two-dimensional optical elements able to control SP propagation were demonstrated. Using a combination of a PSTM with a direct-write lithography technique[17] we can create submicrometer size patterns on the surface of a metal film and measure the SP field redistribution caused by these patterns. An uncoated tapered optical fiber allows us to deliver substantial light power into a diffraction-limited area of the sample near the tip. We are able to ablate submicrometer craters on virtually any opaque surface without damaging a transparent fiber tip. On the other hand, the resolution of our microscope in the PSTM mode depends strongly on the diameter of the uncoated fiber tip: it is not dominated by diffraction. An uncoated fiber tip introduces a relatively small perturbation into the SP field distribution, since the difference $\epsilon_{tip}-1$ between the dielectric constant of the tip and a vacuum is much smaller than the difference between the dielectric constant of the tip and a metal (in the case of silver $\epsilon_{Ag}=-17.9+0.7i$ at $\lambda=633$ nm). A comparison of theoretical and experimentally measured SP field distribution (discussed later in this paper) confirms this conclusion. All these facts make our experimental technique a very reliable tool for a study of the optics of SP's.

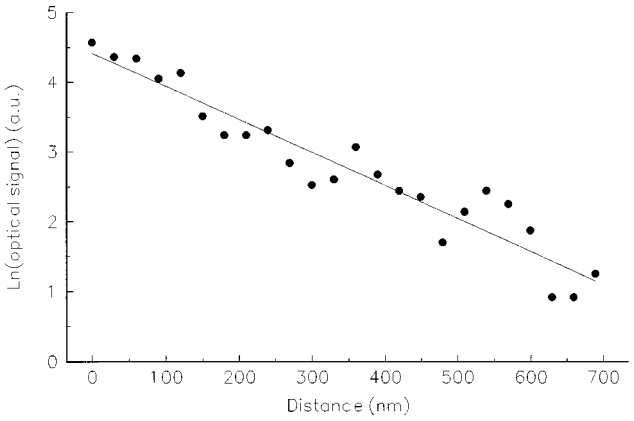

FIG. 2. Dependence of the optical signal on the tip-sample distance.

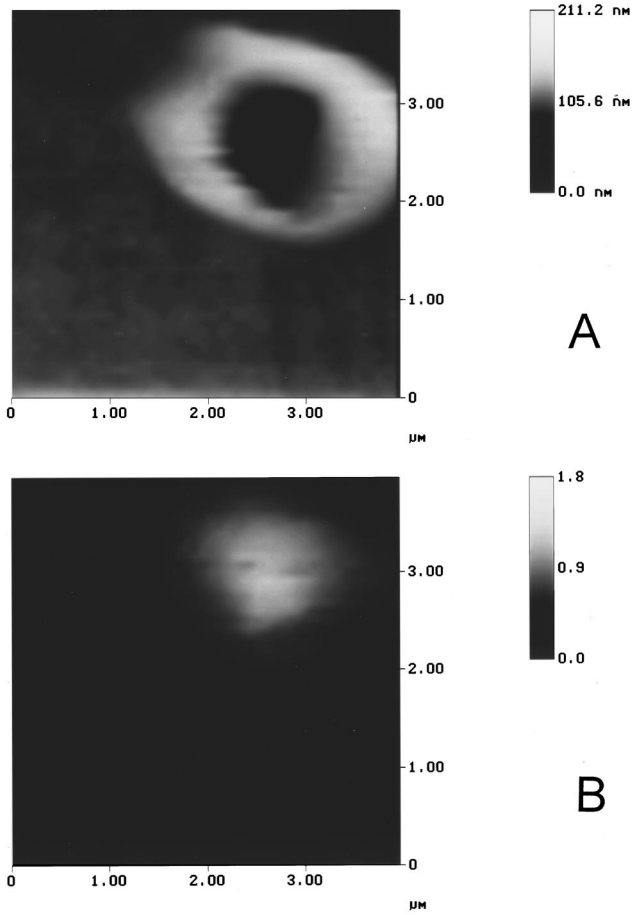

FIG. 3. Topography (a) and optical near-field distribution (b) around a crater created by a UV laser pulse at full energy.

Below we discuss in detail our experimental setup and report experimental observations. In the discussion section we present some model calculations of the SP field distribution around simple defects and compare them with our observations. We present the design of some optical elements that could control SP propagation. Finally, some practical applications of these elements are suggested.

II. EXPERIMENTAL SETUP

In our experiment SP's are excited in an attenuated total reflection (ATR) arrangement[18] on the surface of an 80-nm-

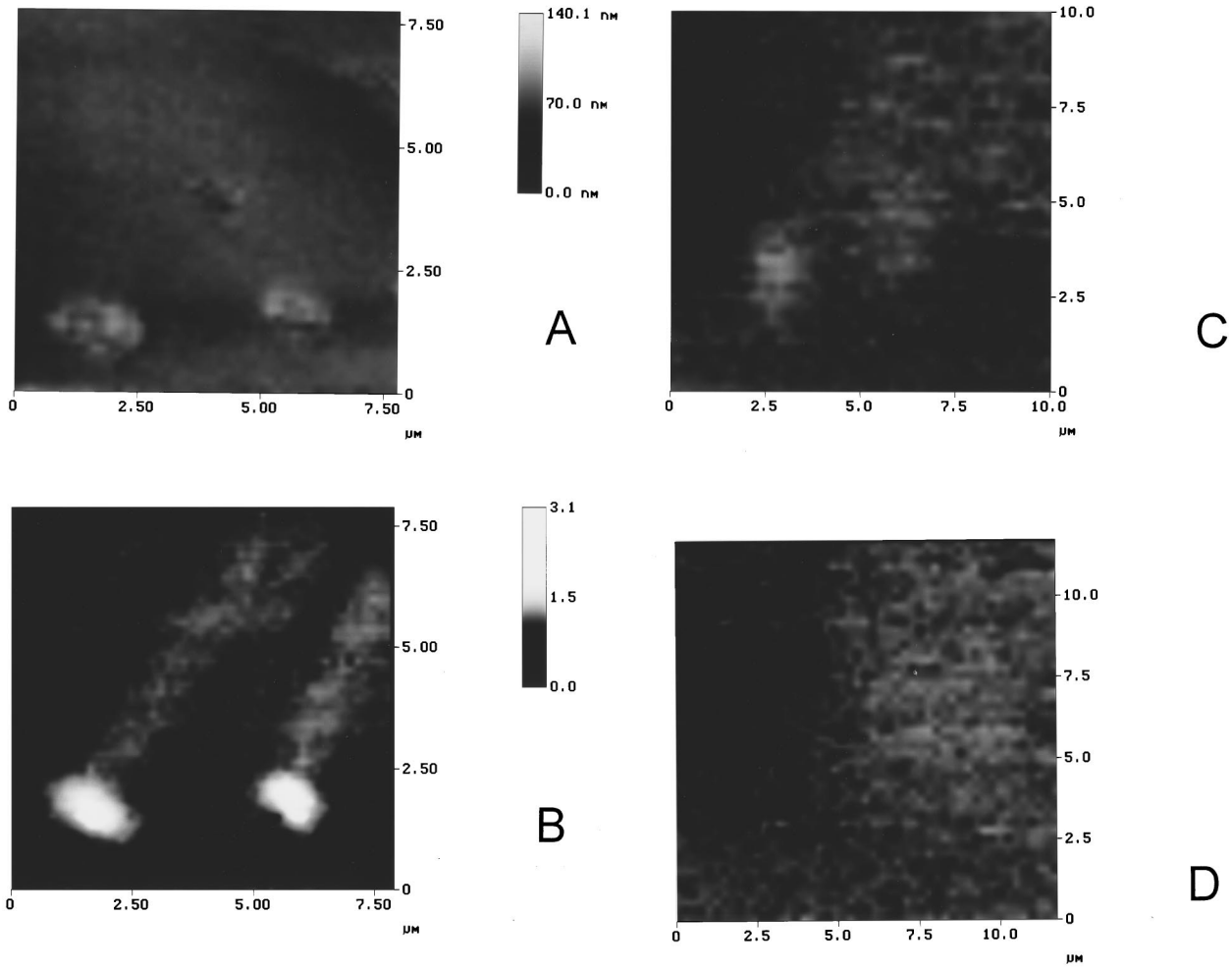

FIG. 4. Topography (a) and optical near-field distribution (b) around two plasmon ''flashlight'' structures. (c) and (d) are far-field images taken at distances 1 and 4 μm from the sample.

thick silver film evaporated onto the hypotenuse face of a right-angle glass prism (Fig. 1). An unfocused P-polarized HeNe laser beam is used for excitation of the SP's. Wave-vector matching to the SP mode at the silver-air interface is achieved when light is internally incident on the silver film at an angle $\alpha=\arcsin\{[\epsilon_{\mathrm{Ag}}/(\epsilon_g\epsilon_{\mathrm{Ag}}+\epsilon_g)]^{1/2}\}=42°$, where ϵ_{Ag} and ϵ_g are the dielectric constants of silver and the glass prism (this value stems from the SP dispersion relation in the thick-film limit[14]). The thickness of the film is a little bit less than the decay length of the SP field into silver, so the coupling of fields between the top and bottom interfaces is sufficient for effective SP excitation. The SP local field is probed with an uncoated, adiabatically tapered fiber tip that is drawn at the end of 200-μm UV fiber by heating it with a CO_2 laser beam in a micropipette puller. The fiber tip can be scanned over the sample surface with a constant tip-surface distance ($\sim$5 nm) using shear force feedback as described elsewhere.[17] Therefore, surface topography can be imaged with a resolution on the nanometer scale, while simultaneously allowing the recording of a near-field optical image corresponding to the distribution of the SP local-field intensity near the film surface. This configuration of a scanning probe microscope is usually called a PSTM.[12]

For the purpose of lithography the free end of the fiber can be connected to the output of a 248-nm excimer laser. The laser power is easily attenuated in order to change the size of defects created in the film. The use of uncoated UV grade tapered fiber and nanosecond pulsed 248-nm excimer laser light allows us to deliver an estimated 200 GW/m^2 UV light power into a tip-sample region smaller then 200×200 nm^2 during a single laser pulse. This power is sufficient for local surface ablation of gold or silver and local melting of silicon without melting of the transparent UV fiber tip.[17] The topographic changes caused by UV irradiation are immediately recorded by the shear force microscope. The developed technique is to some extent similar to STM lithography but is not restricted by the conductance of the sample surface.

III. EXPERIMENTAL RESULTS

The quality of the silver films used in our experiments was good enough to provide a quite homogeneous optical signal distribution over the unmodified surface areas. As a first step, we measured the optical signal dependence on the distance between the tip and the silver film (Fig. 2). The signal exhibits an exponential decay with distance increase: $\mathrm{Ln}(I)=-2\alpha d$ superimposed on a small background. This background signal is due to the scattering of SP's into photons over the entire illuminated film area. The value of the exponent ($\alpha=1/416$ nm) is consistent with the angle of SP

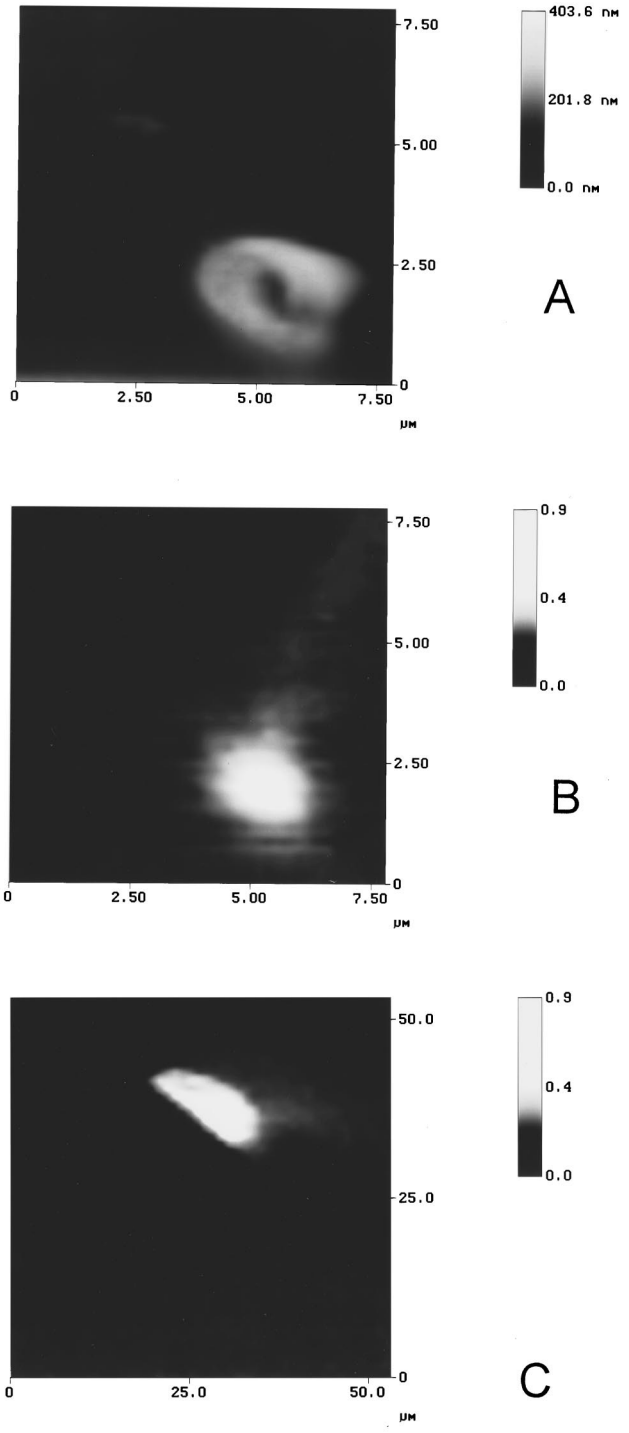

FIG. 5. More complicated defects emitting plasmon beams: topography (a) and optical near-field distribution (b) around an individual defect; (c) is a near-field distribution around a big defect.

excitation. According to theory, the SP field should decay into air with a decay constant $k_z=(k_x^2-\omega^2/c^2)^{1/2}=1/412$ nm, where k_x is the wave vector parallel to the surface.

Below we present images of the optical near-field around *in situ* created defects having different shapes and sizes. These images result from the scattering of the SP field by the defects. They also contain an evanescent component of the totally internally reflected HeNe laser beam used for the excitation of SP's. But this evanescent component does not propagate along the surface, so one can distinguish its contribution from the contribution of SP field scattering. It is important to mention that the contrast of each image is determined internally by scaling the difference between the maximum and minimum of the detected signals to the maximum number of gray levels in the image. A comparison between images therefore needs to be performed with care.

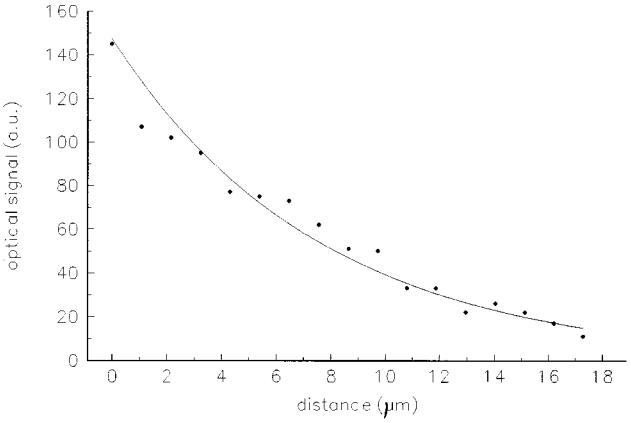

FIG. 6. Cross section of the optical signal in the plasmon beam in Fig. 5(c).

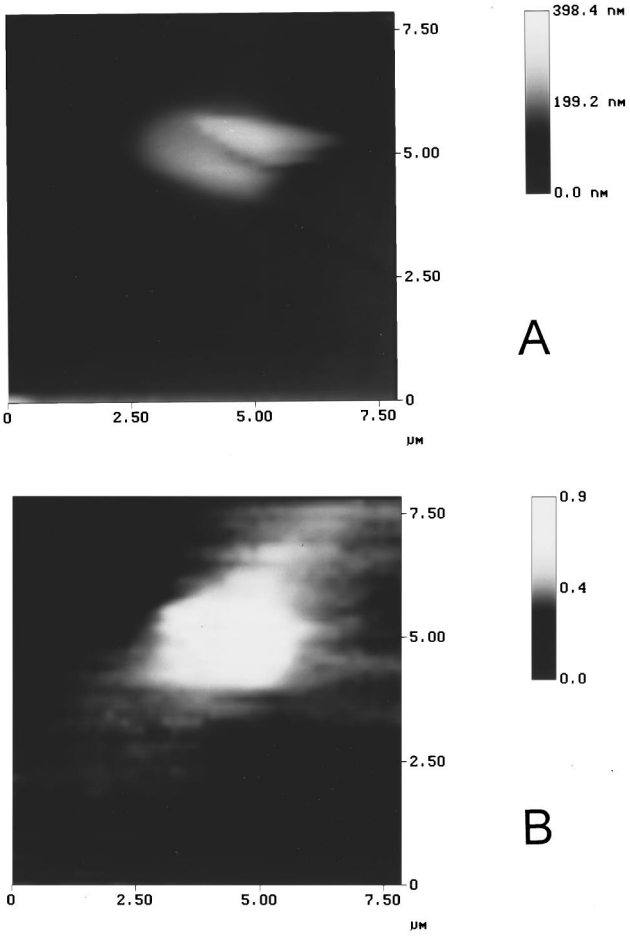

FIG. 7. Topography (a) and optical near-field distribution (b) around a surface defect emitting a weaker reflected plasmon beam. A stronger plasmon beam is emitted in the forward direction.

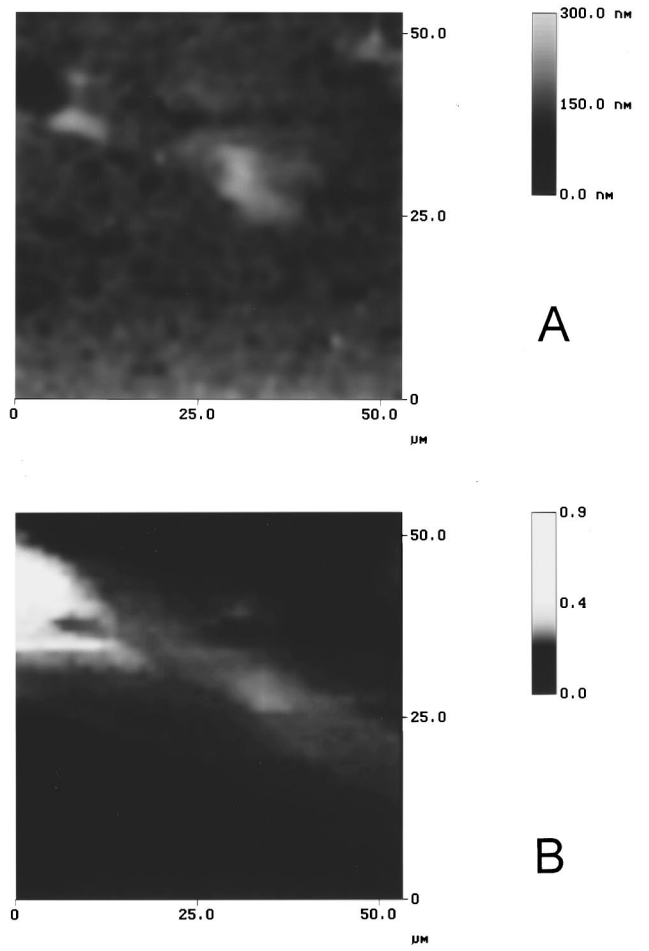

FIG. 8. Scattering of a plasmon beam emitted from a surface defect in the top left corner of the image by another surface defect. As usual, images (a) and (b) are the topography and the near-field distribution, respectively.

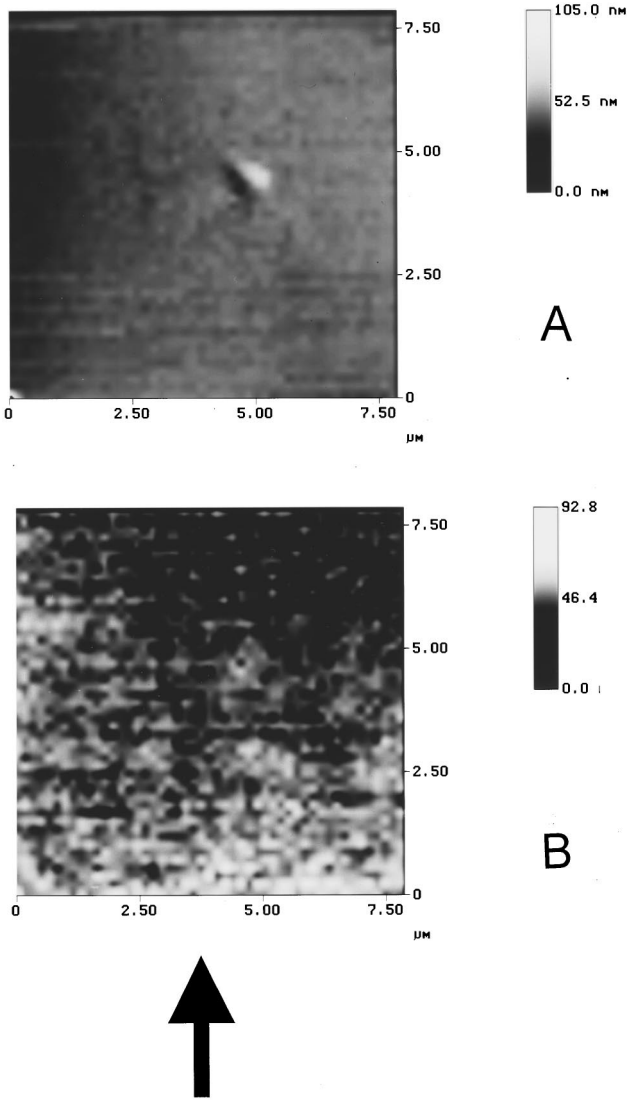

FIG. 9. Topography (a) and optical near-field distribution (b) around smaller defects created at around $\frac{1}{2}$ of the initial power. The direction of plasmon propagation is shown by the arrows. Shadows are seen behind the defects.

At maximum laser power ($\sim$1 nJ per pulse measured in the far field of the tip) a single nanosecond UV pulse delivered to the silver film surface by the uncoated tapered fiber was able to ablate a hole through the 80-nm-thick film. The topography of such a defect [Fig. 3(a)] looks like a large crater with an approximately 0.5-μm hole in the middle. The optical near-field distribution [Fig. 3(b)] has a strong maximum around the hole because the glass prism surface is almost clear of metal in the hole and we see the near field of the totally internally reflected HeNe laser beam used for the excitation of SP's. By attenuating the UV laser pulse power we are able to make craters of shallower depth and smaller diameter. At low power craters may even disappear and we observe a ''hill'' at the irradiated site. Such hills created at approximately $\frac{3}{4}$ of the initial power are shown in Fig. 4. Strong maxima of the optical near field are again seen around these hills. The surprising feature of the near-field image in Fig. 4(b) is the appearance of quite strong and narrow beams (their width is around 1 μm) shining from the hills in the direction determined by the HeNe laser beam used for SP excitation. These ''beams'' are localized within the surface. The near-field intensity seems not to change significantly along the 7-μm length of the left ''beam'' visible in the image. On the other hand, a far-field image taken 7 μm away from the surface is completely dark on the same half-tone scale. A number of images taken at intermediate distances show the spreading and exponential attenuation of the beam ''brightness'' with increasing distance from the surface. Some of them are shown in Figs. 4(c)–4(d). (Note, however, that the contrast for both images is internal and not relative to each other.) Evidently, in the near-field image [Fig. 4(b)] we see surface-plasmon beams shining from the peaks of the optical near-field around the hills. We like to call these structures plasmon ''flashlights.'' Our experience shows that the appearance of a plasmon beam is a rather common features of an optical-field distribution near surface defects in the ATR geometry. In Fig. 5 one can see some other images showing plasmon beams. If the defect has a complicated shape as in Fig. 5(c) the plasmon beam can shine from some region of the defect. The cross section (Fig. 6) of the plasmon beam in this image shows the lateral exponential decay of the SP field intensity with the distance from the source of the beam. The value of the SP propaga-

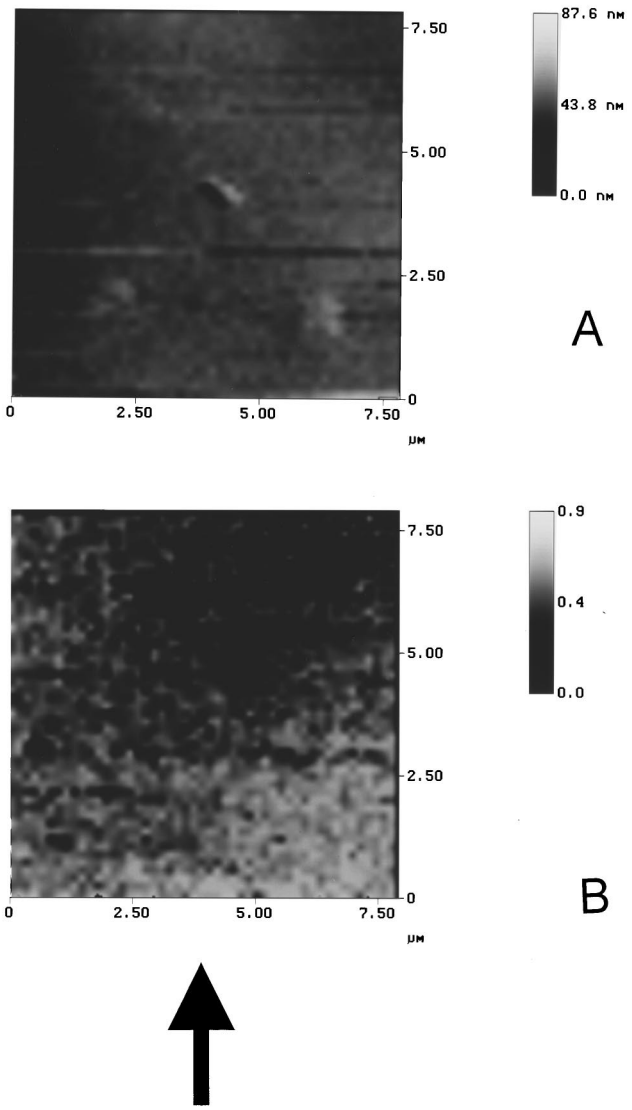

FIG. 10. Topography (a) and optical near-field distribution (b) around three surface defects.

tion length equals 9.1 μm in this case. This value is close to the 13.2-μm value reported in Ref. 14 yet is much smaller than the theoretically estimated propagation length 42.4 μm.[14] A possible explanation of this discrepancy is that the image in Fig. 5(c) was recorded using a rather old silver film sample whose surface looked slightly oxidized. The value of the propagation length derived from the image in Fig. 4(b) taken using a freshly prepared silver film equals 30 μm. This number is much closer to the theoretical value.

In some images of surface defects emitting SP beams one can see not only a forward beam but also a weaker beam emitted in the backward direction (Fig. 7). This means that a ''plasmon mirror'' can be created as another prototype surface optical element. A plasmon beam from one defect can be directed onto another one, as is the case in Fig. 8. One can see a large defect in the top left corner of the image that emits a wide plasmon beam. This beam is scattered by another defect in the middle of the field of view. This experiment shows that one can deal with plasmon ''flashlights'' in the manner that is very similar to the operation of usual three-dimensional light sources.

Attenuation of the UV power during the lithography process allows us to create smaller surface defects and study plasmon scattering by these defects. The results of these studies are shown in Figs. 9 and 10. The UV power used to create these smaller defects was approximately $\frac{1}{2}$ of the initial power. We cannot see bright near-field maxima around these defects any more. Instead, we see prominent shadows behind the defects (the direction of plasmon propagation is shown by the arrows). Two characteristic features of these figures emerge. First, the sources of the shadows appear to be larger in the near-field images than in the topographic ones (a comparison of these images with the near-field image in Fig. 4(b) shows that this effect does not stem from the resolution of the near-field images). Second, for different defects the shadows have different, but still large, angular widths. The approximately 90°-angular widths cannot be accounted for by diffraction. The diffraction angle can be easily estimated from the uncertainty principle: $\beta \sim \delta k_{pl}/k_{pl} \sim \lambda_{pl}/(2\pi d)$, where $\lambda_{pl}=590$ nm is a plasmon wavelength and d is the size of a scatterer. A micrometer size scatterer gives diffraction angle values on the order of 5°. This value is consistent with the rather small visible width of the SP beams from the plasmon ''flashlights'' in Fig. 4(b). Another interesting feature is an apparent difference in the ability to scatter SP field at hills and dips of similar geometrical size. Looking at Fig. 10 one can notice three defects of about the same lateral size. Two of them are shallow hills. The third is a dip of about the same vertical size. The hills seem not to affect the SP propagation at all. On the other hand, the dip gives a distinct angular shadow. In the next part of the paper we propose an explanation for these phenomena. We have used these phenomena to create another simple two-dimensional optical element which we call a ''beam stop.''[16] A number of defects were created along a single line on the surface of a silver film (Fig. 4 in Ref. 16). The near-field image shows some increase in the optical field around the defects and a prominent dark shadow behind the line of defects. Thus, an effective optical shield has been created that does not allow plasmons to pass by.

IV. DISCUSSION

The scattering of SP's by surface defects has been considered in numerous theoretical papers. A recent paper by Pincemin *et al.*[19] contains a good overview of the research in this field. Generally this problem has no analytical solution. Numerically it has been solved for a limited number of experimental geometries. No comparison between such calculations and experimental near-field data has been carried out. Unfortunately, we have not found in the literature any result of numerical calculations that could be directly applied to our observations. Nevertheless we propose two simple models that allow us to understand our results and compare them with theoretical predictions.

The plasmon flashlight phenomenon can be understood directly from the Huygens-Fresnel principle. Let us consider an array of ten secondary sources of SP circular waves (Fig. 11) equally spaced along a 2-μm line. The resulting SP field distribution is given by the expression

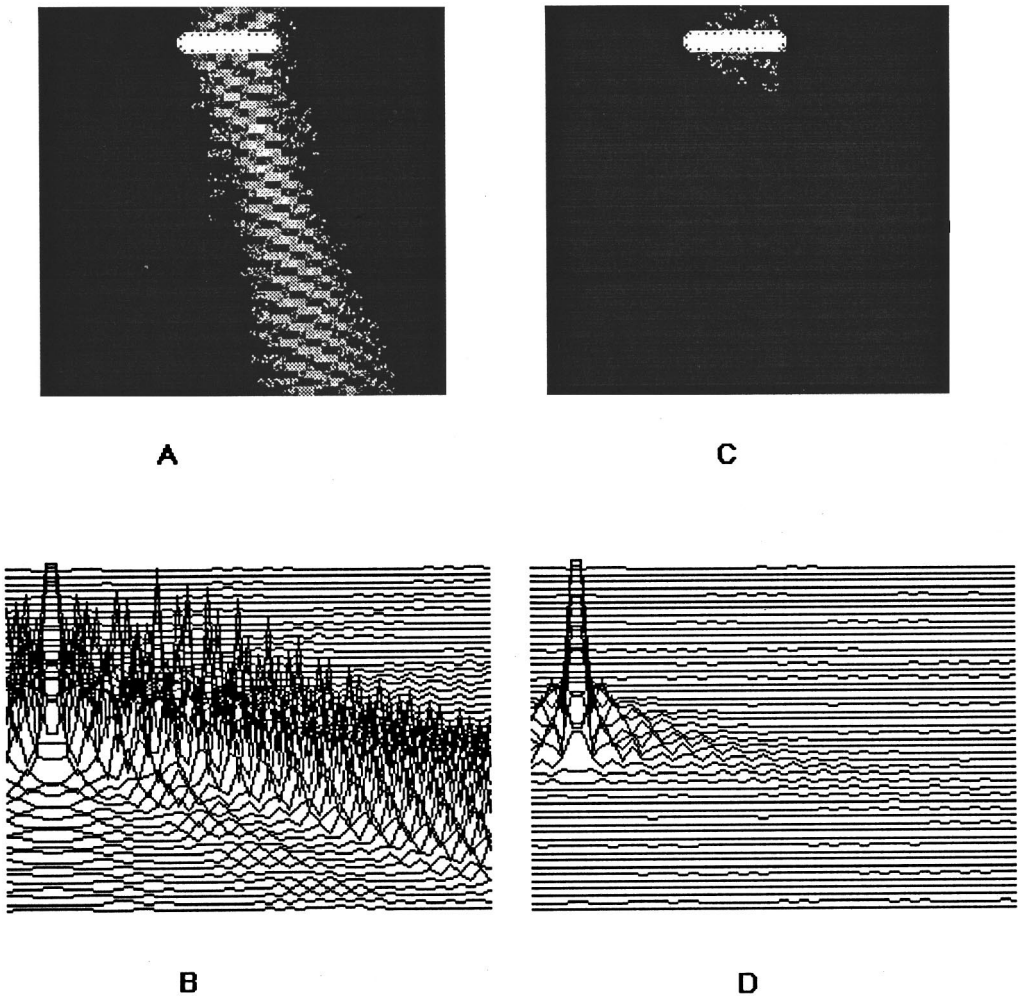

FIG. 11. Field distribution from a 2-μm-long array of point sources in two-dimensional (a), (b) and three-dimensional (c),(d) cases. A pronounced SP beam appears for a two-dimensional field distribution. Horizontal size is 10×10 μm. Halftone views and line scan views are presented.

$$I\sim\left(\sum_n e^{i(kr_n+\phi_n)}/r_n^{1/2}\right)^2, \tag{1}$$

where r_n is the distance between the point of observation and the nth secondary source. This SP field distribution is shown in Fig. 11(a), 11(b) for the case where the phases of secondary sources change linearly with n. A plasmon beam similar to the one in Fig. 5(b) is clearly visible in the half-tone representation. It appears that the primary reason for the beam existence is a weak $\sim r^{-1/2}$ distance dependence of the fields from individual point sources of circular SP waves. For a comparison, the field distribution from the same source calculated using the bulk r^{-1} distance dependence is shown in Figs. 11(c), 11(d). No prominent beam appears in this case. We believe that the strong maxima of the optical near field observed in Figs. 4(b) and 5(b) can be represented by the arrays of secondary sources of SP circular waves. The phase shift between the secondary waves is due to the angular illumination of the defects by the He-Ne excitation laser. It results in the plasmon beam shining in the direction of the incoming beam of HeNe laser. The enhancement of the near field around the defects should be calculated from the exact theory. The main factors contributing to the enhancement are a ''lightning rod effect,'' which leads to field enhancement near the prominent hills on the silver film, and larger photon tunneling through the thinner regions of the film.

Figure 12 represents our modeling of data shown in Fig. 4. Two arrays of secondary sources similar to the one discussed in the previous paragraph are positioned at different distances from each other. Figure 12(c) demonstrates a very close resemblance to Fig. 4(b). It is really a surprising result that two plasmon flashlight structures can be positioned within a few micrometers from each other giving rise to distinctly separate plasmon beams. One can envision numerous applications of these structures in sensor arrays. Each plasmon beam could probe the surface chemistry in a very localized region. Based on the success of our plasmon beam modeling we suggest some optical elements that could control SP propagation. One could think of focusing mirrors or lenses consisting of surface defects similar to ones in Fig. 4. Some examples of these optical elements are shown in Fig. 13. A curved defect described (in polar coordinates) by the expression $R(\alpha)=2F/(1+\cos\alpha)$ would be a perfect focusing mirror with focal length F: $R(\alpha)$ is a solution of the equation $kR(\alpha)+\phi(\alpha)=\text{const}$ [where $\phi(\alpha)=kR(\alpha)\cos(\alpha)$] for the positions of the point sources that would direct reflected secondary SP waves to be exactly in phase at some particular focal point. A curved defect as shown in Fig. 13(b), which

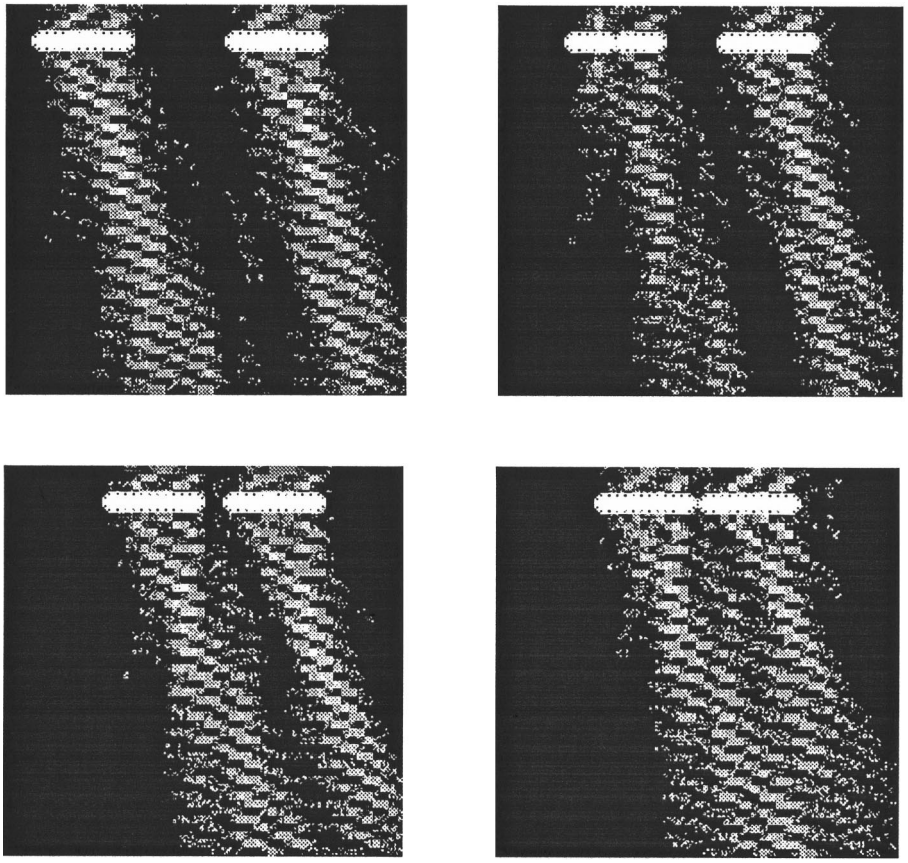

FIG. 12. Numerical modeling of two plasmon flashlights at different distances from each other. Horizontal size is 10×10 μm.

consists of two parts of this focusing mirror positioned next to each other should have two focal points. These calculations are justified by the observation of a ''plasmon mirror'' in Fig. 7. Another possibility is to create a focusing lens using a zone plate principle. Figure 13(c) represents the field distribution of such an element. The defects are positioned on a circle of radius R in order to compensate for the distance dependence of the field in a circular wave. The angular position of the nth point SP source is given by the expression $kR-kR\cos(\alpha_n)=2\pi n$. All these optical elements could find numerous applications in integrated optics.

Let us now discuss our data concerning the SP scattering by smaller defects. The simplest explanation of the observed discrepancy between the visible sizes of the shadow sources in the near-field and topographic maps could be that the actual size of the scatterers is not the one that is seen in the surface topographic map. The bulk structure of the silver film can be deformed around the surface defect. Also the chemical composition of the surface oxide layer (and/or absorbed layer) could be changed under UV irradiation on a much larger scale than is apparent in the visible size of the defect. Precise control of these parameters would require experiments under ultrahigh-vacuum conditions. But, there is strong theoretical evidence that the visible size of even a point scatterer in the near-field map may be on the order of some micrometers. Let us imagine a point defect on an otherwise ideally flat metal film surface. This defect is irradiated by a plane surface-plasmon wave. The defect breaks translation symmetry of the film surface. The SP wave can transfer part of its momentum to the defect and decay into a photon. Consider the cross section of the point defect for such a process. This point defect can be Fourier decomposed into a set of diffraction gratings with periods from zero to infinity (in reality, the upper limit is the inverse atomic size). Since SP scattering is a linear process we can treat the SP interaction with each diffraction grating separately. Each grating can change the momentum of a plasmon by a multiple of its inverse period. Most probably the plasmon momentum will change by only one inverse grating period. If the inverse grating period is smaller than the difference between the momentum of plasmon and the momentum of photon, then plasmon decay will not happen. Hence, only grating with sufficiently large inverse periods will contribute to the cross section of SP decay into photons. In order to find this cross section we should cutoff the Fourier spectrum of the defect at wave vectors less then the difference between the plasmon and photon wave vectors ($k_{\rm pl}-k_{\rm ph}$) and perform an inverse Fourier transformation. Such a procedure gives an effective cross section $s\sim1/(k_{\rm pl}-k_{\rm ph})$. This cross section is $s\sim1.6$ μm at HeNe laser wavelengths. This value is consistent with the effective sizes of the shadow sources in Fig. 9(b).

Another effect that might produce a shadowlike phenomenon around a surface defect is attenuated energy transfer from the He-Ne laser excitation beam into the SP's. Resonant excitation of SP's is happening because of the phase matching between the SP and the HeNe beam in the glass prism. The phase-matching length L is determined by the angular width of the SP resonance (see Fig. 1) which is usually on the order of $\delta\alpha\sim1°$: $\delta k_{\rm pl}L\sim\delta\alpha k_{\rm pl}L\sim1$. This gives a value of the phase-matching length on the order of $L\sim5$

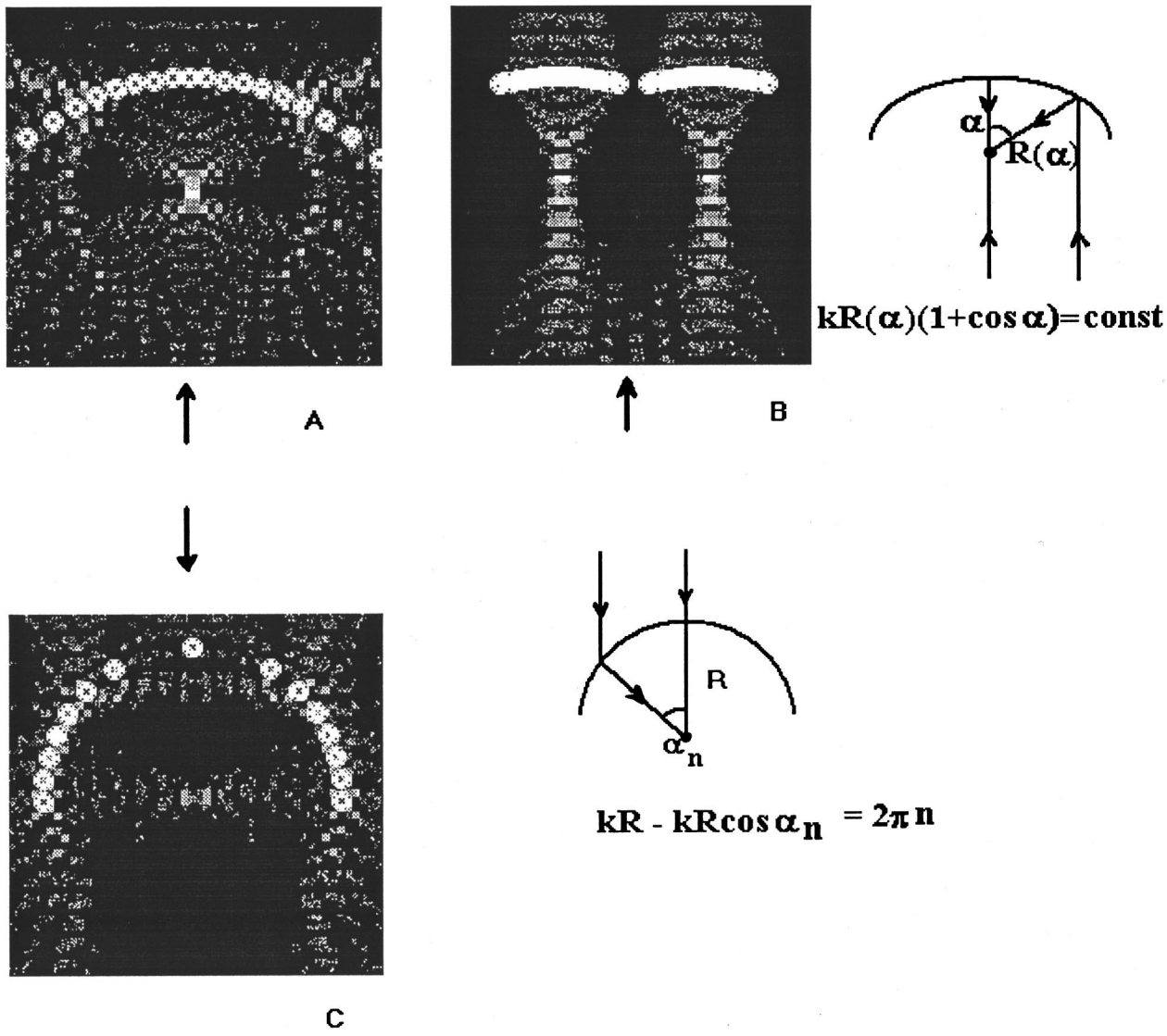

FIG. 13. Numerical modeling of plasmon mirrors (a),(b) and a plasmon lens (c). Horizontal size is 10×10 μm.

μm. A surface defect could worsen this phase matching and cause smaller energy transfer in to the SP's. A smaller intensity of the SP field would look like a shadow behind the defect. The two effects discussed above lead to essentially the same effective size of the shadow source. We believe both effects contribute to the observed field distribution. Unfortunately, neither of these effects could be responsible for the angular shape of the shadows and an apparent difference between SP scattering by shallow hills and dips.

The most probable reason for shadows to have an angular shape is refraction. As we have discussed earlier, the SP interaction with a surface defect can be decomposed into interactions with separate gratings that constitute the Fourier spectrum of a defect. Interaction with gratings that have periods much smaller than $2\pi/(k_{\mathrm{pl}}-k_{\mathrm{ph}})$ leads to SP decay into photons. Interaction with the rest of the gratings can be treated like two-dimensional optics: a plasmon will remain a plasmon after the interaction. Thus, we can talk about SP refraction.

It is relatively easy to introduce an effective refractive index for a shallow dip or hill that scatters a SP wave. The dispersion relation for the SP in the three-media air-metal-glass system can be written as follows:[20]

$$(\epsilon_1/k_1+\epsilon_2/k_2)(\epsilon_2/k_2+\epsilon_3/k_3)+(\epsilon_1/k_1-\epsilon_2/k_2)(\epsilon_/k_2-\epsilon_3/k_3)e^{-2k_2d_2}=0, \tag{2}$$

where $k_n=(k_x^2-\omega^2\epsilon_n/c^2)^{1/2}$, and $n=1,2,3$ denotes glass, silver film, and air, respectively. After some transformations the dispersion law can be rewritten in the more explicit form:

$$\omega=k_xc[(\epsilon_2+1)/\epsilon_2]^{1/2}(1+Ae^{-2k_2d_2}), \tag{3}$$

where

$$A=2\epsilon_2\frac{[(-\epsilon_1\epsilon_2+\epsilon_2-\epsilon_1)^{1/2}+i\epsilon_1]}{\{(\epsilon_2^2-1)[(-\epsilon_1\epsilon_2+\epsilon_2-\epsilon_1)^{1/2}+i\epsilon_1]\}}\sim0.11 \tag{4}$$

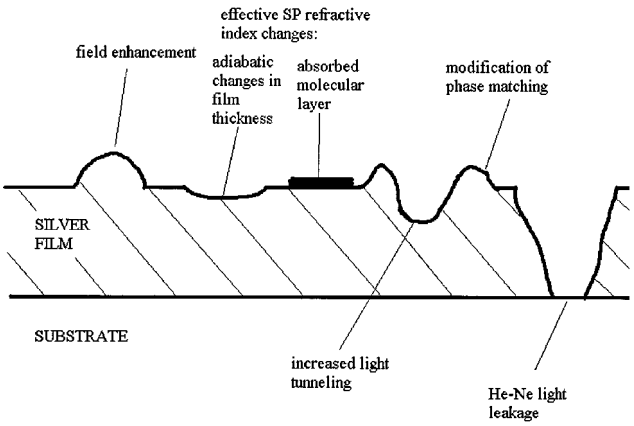

FIG. 14. Summary of different physical mechanisms affecting surface-plasmon field distribution.

(here we assume that the thickness of the silver film is large enough that $e^{-2k_2d_2} \ll 1$). As we can see, the phase velocity of SP depends on the thickness of the silver film. The SP's are faster in the areas where the thickness of a film is smaller. The effective refractive index of a shallow defect can be written as follows:

$$n = V_0/V = 1 + A(e^{-2k_2d_0} - e^{-2k_2d}), \tag{5}$$

where V is a SP phase velocity at thickness d and V_0 is a SP phase velocity in unmodified areas of a silver film with a thickness d_0. Numerical analysis of this expression shows that in our experiments (with $d_0 = 80$ nm) the effective refractive index n varies within the range 0.89–1.0001. For shallow hills $n > 1$ and the changes in n are negligible, while shallow dips have $n < 1$. This results agrees qualitatively with our observations in Fig. 10. Shallow hills should have much less of an effect on the SP propagation than shallow dips. Evidently, shallow dips act as negative lenses. This results in the angular shape of shadows.

Similar effective refractive indices could be assigned to areas of the silver film where the composition of an absorbed layer is modified. Sometimes the presence of an absorbed layer could lead to appearance of additional SP modes.[21] But in many cases the presence of a few molecular monolayers on the surface of a metal film leads only to a shift in the SP phase velocity.[22] In terms of effective refractive index this shift can be expressed as follows:

$$n = 1 + (\epsilon_a - 1)/[\epsilon_a(-\epsilon_{Ag} - 1)^{1/2}] \times 2\pi d_a/\lambda, \tag{6}$$

where ϵ_a is a dielectric constant and d_a is the thickness of an absorbed layer (here we assume that $\epsilon_a \ll \epsilon_{\mathrm{Ag}}$). According to Ref. 23 four monolayers of cadmium arachidate gives a shift in the SP phase velocity which corresponds to $n = 1.033$. The potential consequence of this result for our experiment is that possible modification of an absorbed layer by an UV light pulse during defect creation could cause refraction of SP's around the defect. On the other hand, this effect can be used to create simple optical elements for SP field redistribution such as lenses or prisms. A triangular region of the silver film covered with a layer of molecules such as cadmium arachidate would act like a prism on a propagating SP beam. One could calculate the dispersion of this prism by taking into account the dispersion of ϵ_{Ag} and ϵ_a. This has the same order of magnitude as the dispersion of any bulk prism. The dispersion of such optical elements can be used in multichannel chemical sensors and biosensors.

Figure 14 summarizes our discussion of different effects that influence the SP field distribution near surface defects. A change of metal film thickness and the local surface tilt cause the modification of the phase matching between the He-Ne laser light and SP's. Some sharp surface ''hills'' and holes through the film can cause strong-field enhancement in their vicinity. These effects influence the electromagnetic field distribution in close proximity to these defects. One needs to use an exact theory to describe these ''near-field'' effects.

The SP ''far-field'' distribution is much easier to understand using such simple concepts as the Huygens-Fresnel principle and effective SP refractive index. One can replace strong maxima of the near field around the hills and the holes with secondary SP sources. Adiabatic changes in film thickness and local variations in the absorbed molecular layer can be described by an effective refractive indices. Then the nature of SP propagation can be treated as a two-dimensional optics problem.

V. CONCLUSIONS

In summary, we have constructed a combined PSTM/direct-wire lithography setup that has allowed us to study the scattering of surface plasmons by individual defects, while continuously adjusting their shapes and sizes. The use of an uncoated fiber tip as a local probe causes much less perturbation of the SP field as compared to other scanning probe techniques such as STM, AFM, or near-field optical microscopy with metal-coated tips.

Surface defects that emit micrometer wide SP beams (plasmon flashlights) have been observed. This phenomenon has been explained using the Huygens-Fresnel principle. Scattering and refraction of SP field by smaller surface defects has also been studied. The concept of effective refractive index has been introduced for two classes of surface defects: shallow hills or dips, and areas covered with a layer of absorbed molecules. This concept allows us to achieve a qualitative understanding of SP field redistribution by defects, which is otherwise a complicated theoretical problem without an analytical solution.

Some simple optical elements able to govern SP field propagation have been suggested. We believe our technique has the potential to create analogs of any three-dimensional optical devices in two dimensions. Similar techniques can be used not only in the two-dimensional optics of surface plasmons on metal surfaces but also in the optics of any surface waves on semiconductors and dielectrics. Plasmon flashlights in combination with other SP optical elements could have numerous potential applications in multichannel chemical sensing, biosensing, and integrated optics.

ACKNOWLEDGMENTS

We would like to acknowledge helpful discussions with Julius Goldhar and Saeed Pilevar.

[1] *Surface Polaritons*, edited by V. M. Agranovich and D. L. Mills (North-Holland, Amsterdam, 1982).
[2] H. Raether, *Surface Plasmons*, Springer Tracts in Modern Physics Vol. 111 (Springer, Berlin, 1988).
[3] G. N. Zhizhin *et al.*, in *Surface Polaritons* (Ref. 1), p. 122.
[4] B. Liedberg, C. Nylander, and I. Lundstr, Sens. Actuators **4**, 299 (1983).
[5] E. Yeatman and E. A. Ash, Electron. Lett. **23**, 1091 (1987); B. Rothenhausler and W. Knoll, Nature (London) **332**, 615 (1988).
[6] R. Moller *et al.*, J. Vac. Sci. Technol. B **9**, 506 (1991); N. Kroo *et al.*, Europhys. Lett. **15**, 289 (1991).
[7] M. Specht, J. D. Pedarnig, W. M. Heckl, and T. W. Hansch, Phys. Rev. Lett. **68**, 476 (1992).
[8] R. W. Rendell and D. J. Scalapino, Phys. Rev. B **24**, 3276 (1981).
[9] R. B. G. De Hollander, N. F. van Hulst, and R. P. H. Kooyman, Ultramicroscopy **57**, 263 (1995); Y.-K. Kim, J. B. Ketterson, and D. J. Morgan, Opt. Lett. **21**, 165 (1996).
[10] *Near Field Optics*, edited by D. W. Pohl and D. Courjon (Kluwer, The Netherlands, 1993).
[11] B. Hecht *et al.*, in *Photons and Local Probes*, edited by O. Marti and R. Moller (Kluwer, The Netherlands, 1995), p. 93; Phys. Rev. Lett. **77**, 1889 (1996).
[12] R. C. Reddick, R. J. Warmack, and T. L. Ferrel, Phys. Rev. B **39**, 767 (1989); D. Courjon, K. Sarayeddine, and M. Spajer, Opt. Commun. **71**, 23 (1989); F. de Fornel *et al.*, Proc. SPIE **77**, 1139 (1989).
[13] O. Marti *et al.*, Opt. Commun. **96**, 225 (1993); P. M. Adam *et al.*, Phys. Rev. B **48**, 2680 (1993).
[14] P. Dawson, F. de Fornel, and J.-P. Goudonnet, Phys. Rev. Lett. **72**, 2927 (1994).
[15] S. I. Bozhevolnyi, I. I. Smolyaninov, and A. V. Zayats, Phys. Rev. B **51**, 17 916 (1995).
[16] I. I. Smolyaninov, D. L. Mazzoni, and C. C. Davis, Phys. Rev. Lett. **77**, 3877 (1996).
[17] I. I. Smolyaninov, D. L. Mazzoni, and C. C. Davis, Appl. Phys. Lett. **67**, 3859 (1995); I. I. Smolyaninov *et al.*, in *Conference on Lasers and Electro-Optics*, OSA Technical Digest Series (OSA, Washington, D.C., 1996), Vol. 9, p. 253.
[18] E. Kretschmann and H. Raether, Z. Naturforsch. A **23**, 2135 (1968).
[19] F. Pincemin, A. A. Maradudin, A. D. Boardman, and J.-J. Greffet, Phys. Rev. B **50**, 15 261 (1994).
[20] C. A. Ward *et al.*, J. Chem. Phys. **62**, 1674 (1975).
[21] V. M. Agranovich, Zh. Éksp. Teor. Fiz. **77**, 1124 (1979) [Sov. Phys. JETP **50**, 567 (1979)].
[22] F. Abeles and T. Lopez-Rios, in *Surface Polaritons* (Ref. 1), p. 252.
[23] J. G. Gordon and J. D. Swalen, Opt. Commun. **22**, 374 (1977).